RESEARCH ARTICLE

Actomyosin-mediated cellular tension promotes Yap nuclear translocation and myocardial proliferation through α5 integrin signaling

Xiaofei Li[1], Callie McLain[1], Michael S. Samuel[2,3], Michael F. Olson[4] and Glenn L. Radice[1,*]

ABSTRACT

The cardiomyocyte phenotypic switch from a proliferative to terminally differentiated state results in the loss of regenerative potential of the mammalian heart shortly after birth. Nonmuscle myosin IIB (NM IIB)-mediated actomyosin contractility regulates cardiomyocyte cytokinesis in the embryonic heart, and NM IIB levels decline after birth, suggesting a role for cellular tension in the regulation of cardiomyocyte cell cycle activity in the postnatal heart. To investigate the role of actomyosin contractility in cardiomyocyte cell cycle arrest, we conditionally activated ROCK2 kinase domain (ROCK2:ER) in the murine postnatal heart. Here, we show that α5/β1 integrin and fibronectin matrix increase in response to actomyosin-mediated tension. Moreover, activation of ROCK2:ER promotes nuclear translocation of Yap, a mechanosensitive transcriptional co-activator, and enhances cardiomyocyte proliferation. Finally, we show that reduction of myocardial α5 integrin rescues the myocardial proliferation phenotype in ROCK2:ER hearts. These data demonstrate that cardiomyocytes respond to increased intracellular tension by altering their intercellular contacts in favor of cell–matrix interactions, leading to Yap nuclear translocation, thus uncovering a function for nonmuscle myosin contractility in promoting cardiomyocyte proliferation in the postnatal heart.

KEY WORDS: Rho-associated kinase, Nonmuscle myosin, Heart, Cardiomyocyte, Cell adhesion, Cadherin, Integrin, Adherens junctions, Focal adhesions, Fibronectin, Yap, Mouse

INTRODUCTION

The neonatal mammalian heart is capable of substantial regeneration following injury; however, this regenerative capacity largely disappears in the first week after birth (Porrello et al., 2011, 2013). As such, the adult human heart does not have an effective mechanism to regenerate the cardiomyocytes (CMs) lost following a heart attack. Instead, the lost muscle is replaced by the excessive deposition of extracellular matrix (ECM), which together reduces both systolic and diastolic left ventricular (LV) functions of the heart and often leads to heart failure. Thus, a better understanding of the molecular mechanisms controlling CM proliferation is required in order to identify novel targets that will stimulate cardiac regeneration following myocardial infarction.

The Rho-associated coiled-coiled containing protein serine/threonine kinases ROCK1 and ROCK2 are downstream effectors of the Rho subfamily of small GTPases (Hartmann et al., 2015; Noma et al., 2006; Shimokawa et al., 2016). As a key regulator of intracellular contractility, ROCK1/2 allows cells to respond to mechanical cues from the tissue microenvironment. Evidence from animal studies indicate an important role for ROCK in cardiac morphogenesis and in adult heart pathophysiology (Shi et al., 2011). Pharmacological inhibition of ROCK during early chick and mouse embryogenesis has been shown to cause defects in cardiac morphogenesis (Wei et al., 2001). Consistent with this finding, simultaneous deletion of both ROCK1 and ROCK2 in the heart using a cardiac-specific αMHC-Cre transgene causes embryonic lethality (Shi et al., 2019). Interestingly, cardiac-restricted knockout of ROCK2 using the αMHC-Cre transgene (ROCK2 CKO mouse model) did not result in a cardiac phenotype under basal conditions (Okamoto et al., 2013; Sunamura et al., 2018). However, following angiotensin II treatment or transverse aortic constriction ROCK2 CKO mice exhibited less cardiac hypertrophy, reduced end-diastolic wall thickness, and decreased LV mass compared with control littermates, supporting the idea that ROCK2 is required for CMs to respond to mechanical stimuli. Using a ROCK dominant-negative transgenic model (ROCK DN), endogenous ROCK activity was blocked in embryonic CMs, resulting in disruption of sarcomeres and reduced CM proliferation (Bailey et al., 2019), although no molecular mechanism was established to account for the decreased CM proliferation. These *in vivo* studies demonstrate the requirement for ROCK2 signaling in cardiac development and cardiac remodeling following mechanical stress, but its specific role in postnatal CM maturation remains poorly defined.

ROCK mediates the phosphorylation of myosin regulatory light chains leading to increased myosin ATPase activity, thus stimulating actomyosin contractility. Nonmuscle myosin IIB (NM IIB) is the primary NM isoform expressed in heart muscle. As CMs mature after birth, nonmuscle myosin activity decreases and it is reactivated in response to mechanical stress in the adult heart, e.g. after myocardial infarction (Ma and Adelstein, 2012; Pandey et al., 2018). Germline knockout of NM IIB in mice leads to multiple developmental abnormalities, including cardiac malformations and cardiac hypertrophy resulting in embryonic lethality (Tullio et al., 1997). Notably, defective cytokinesis causes an increased number of enlarged binucleated CMs in the NM IIB mutant hearts, supporting a role for NM IIB in myocardial proliferation (Takeda et al., 2003). Mechanistically, NM IIB actin cross-linking activity is required to generate tension that drives cytokinesis (Ma et al., 2012).

[1]Cardiovascular Research Center, Lifespan Cardiovascular Institute, Rhode Island Hospital, Department of Medicine, Division of Cardiology, Alpert Medical School of Brown University, Providence, RI 02903, USA. [2]Centre for Cancer Biology, an alliance between SA Pathology and the University of South Australia, Adelaide 5000, Australia. [3]Adelaide Medical School, Faculty of Health and Medical Sciences, University of Adelaide, Adelaide 5000, Australia. [4]Department of Chemistry and Biology, Toronto Metropolitan University, Toronto, Ontario, M5B 2K3 Canada.

*Author for correspondence (glenn_radice@brown.edu)

M.S.S., 0000-0001-7880-6379; M.F.O., 0000-0003-3428-3507; G.L.R., 0000-0002-2944-1059

DEVELOPMENT

1

Cardiac-specific NM IIB knockout (αMHC-Cre) mice also exhibit cytokinesis defects; however, the mutant mice survive and go on to develop progressive cardiomyopathy with age (Ma et al., 2009). Taken together, these data indicate the importance of NM IIB in regulating cardiac development and homeostasis, including CM cytokinesis.

The transition from hyperplastic to hypertrophic growth in the postnatal heart is accompanied by dynamic remodeling of cell–cell and cell–ECM adhesive junctions. Specifically, CM α5/β1 integrin-fibronectin (FN; FN1) adhesions decrease after birth and N-cadherin (cadherin 2, CDH2) junctions remodel and accumulate at myocyte termini leading to the formation of a specialized junction called the intercalated disc (ICD) (Vite and Radice, 2014). Establishment of functional cadherin and integrin adhesion complexes require the reorganization and assembly of the actin cytoskeletal network. Modulation of intracellular tension can have different effects on cell–cell and cell–ECM interactions depending on the cellular context (de Rooij et al., 2005; Dzamba et al., 2009; Liu et al., 2010; Martinez-Rico et al., 2010; Shewan et al., 2005). Here, we focus on the effects of cellular tension on the remodeling of myocardial adhesions in the postnatal heart prior to ICD assembly.

We previously reported that altering the linkage between N-cadherin and the actin cytoskeleton by depleting αE-/αT-catenins (CTNNA1/3) caused an increase in RhoA activity, mislocalization of actomyosin contractility, and enhanced CM proliferation in the postnatal mouse heart (Li et al., 2015; Vite et al., 2018). Whether enhanced intracellular tension is responsible for the CM hyperproliferation phenotype in the αE-/αT-catenin mutant mice is unknown. To address this possibility, here we studied the direct effect of activating ROCK2 signaling and consequent actomyosin contractility on CM maturation. We find that inducing actomyosin contractility leads to a rebalancing of myocardial cell–cell and cell–matrix adhesions, with the latter responsible for Yap (Yap1) nuclear translocation and CM proliferation. These results implicate the actomyosin cytoskeleton as a crucial mediator of crosstalk between cadherin and integrins, and show that activating nonmuscle myosin contractility leads to enhanced myocardial cell–FN interactions, which stimulate CM proliferation in the postnatal heart.

RESULTS
ROCK activation increases nonmuscle myosin contractility in the postnatal heart
The temporal expression of NM IIB, nonmuscle myosin light chain 2 (MLC2; MYL2), and active phosphorylated MLC2 (pMLC2) was examined in postnatal hearts of wild-type mice (C57BL/6J) by western blotting (Fig. 1A). NM IIB, which controls tension within the actin cytoskeleton, is activated by phosphorylation of its light chain at Ser19 (pMLC). Both NM IIB levels and MLC2 activity declined after birth (Fig. 1A), consistent with previous report of NM IIB expression in murine heart (Tullio et al., 1997), whereas ROCK2 levels remained constant over the same period. To investigate the effects of actomyosin contractility on CM differentiation and cell cycle arrest, we used a conditionally activated ROCK2:ER mouse model (Samuel et al., 2016), outlined in Fig. 1B. Fusion of the ROCK2 kinase domain with the estrogen receptor (ER) hormone-binding domain generates a ROCK2:ER chimeric protein that is inactive in the absence of ligand, but which can be conditionally activated in vivo by administering the estrogen analog 4-hydroxytamoxifen (Tam) (Rath et al., 2017; Samuel et al., 2016). ROCK2:ER mice were bred with αMHC/Cre mice to generate a cardiac-restricted ROCK2: ER mouse model. Western blot analysis confirmed expression of the

ROCK2:ER fusion protein in ROCK2:ER; αMHC-Cre hearts (Fig. 1D). CM proliferation decreases after postnatal day (P) 4 in mice (Soonpaa et al., 1996). Therefore, to investigate the effects of cellular tension on the transition from hyperplastic to hypertrophic CM growth, mice were administered Tam via intraperitoneal injection for three consecutive days: P5, P6 and P7 (Fig. 1C). On P7, 4 h after the last Tam injection, hearts were harvested for analysis. The kinase ROCK2 is required for RhoA-initiated actomyosin contractility, acting through phosphorylation of substrates including MLC2 and MYPT1 (PPP1R12A). Western blot analysis confirmed increased expression of NM IIB, pMLC2 (Ser19) and pMYPT (Thr696) in ROCK2:ER; MHC-Cre hearts following Tam administration (Fig. 1E). Tam administration alone to wild-type C57BL/6J mice had no effect on actomyosin contractility, as determined by pMLC/MLC expression (Fig. S1). For all subsequent studies, pups were administered Tam as described above. Littermates lacking the Cre transgene (i.e. ROCK2:ER alone) served as controls, and ROCK2:ER; MHC-Cre mice are referred to as 'ROCK'. Actomyosin contractility, as visualized by punctate pMLC immunofluorescence, was higher in P7 ROCK CMs compared with control (Fig. 1F). Consistent with increased nonmuscle myosin contractility, there was more NM IIB along the lateral membrane of ROCK CMs compared with control (Fig. 1G).

Histological analysis did not detect any cellular or morphological abnormalities in the P7 ROCK hearts (Fig. S2). To assess cardiac function, echocardiography was performed on P7 pups. There was no change in LV function as determined by ejection fraction and fraction shortening in the ROCK mice (Fig. S2). Moreover, LV anterior (LVAW) and posterior (LVPW) wall thickness was not changed in the ROCK mice. Thus, temporary (P5-P7) activation of ROCK2 did not perturb cardiac structure or function.

Increased intracellular tension shifts the balance between cell–cell to cell–matrix adhesions
Mechanical equilibrium between cells and tissues is dependent on maintaining a proper balance between cell–cell and cell–ECM interactions (Han and de Rooij, 2016; Mui et al., 2016; Zuidema et al., 2020). To investigate the effects of actomyosin contractility on the crosstalk between cell–ECM and cell–cell interactions, we examined the spatial distribution and expression of α5/β1 integrin (the receptor for FN) and FN in P7 ROCK hearts (Fig. 2A). Increase in α5 integrin expression was accompanied by enhanced extracellular FN matrix along the lateral membrane, consistent with strengthening of myocardial cell–matrix interactions in the ROCK hearts. Integrin-FN binding leads to the formation of FN fibrils that are initially soluble in the detergent deoxycholate (DOC) but are gradually converted into a stable, DOC-insoluble form that comprises the mature matrix (Sechler et al., 1996). Both α5 and FN increased in the DOC-insoluble fraction, consistent with compensatory matrix assembly in response to altered intracellular tension in ROCK-activated CMs (Fig. 2B). At this developmental stage, N-cadherin and α5 integrin exhibited extensive colocalization at the membrane, with the notable exception of enhanced α5 integrin expression at the lateral membrane in the ROCK CMs (Fig. 2C, enlarged images).

Both the cadherin- and integrin-based adhesion systems are linked to the cortical actin cytoskeleton and share common downstream actin regulatory pathways, including the cytoskeletal adaptor protein vinculin. Vinculin regulates cell adhesion by directly binding to actin, stimulating actin polymerization and recruiting actin remodeling proteins in response to intrinsic and
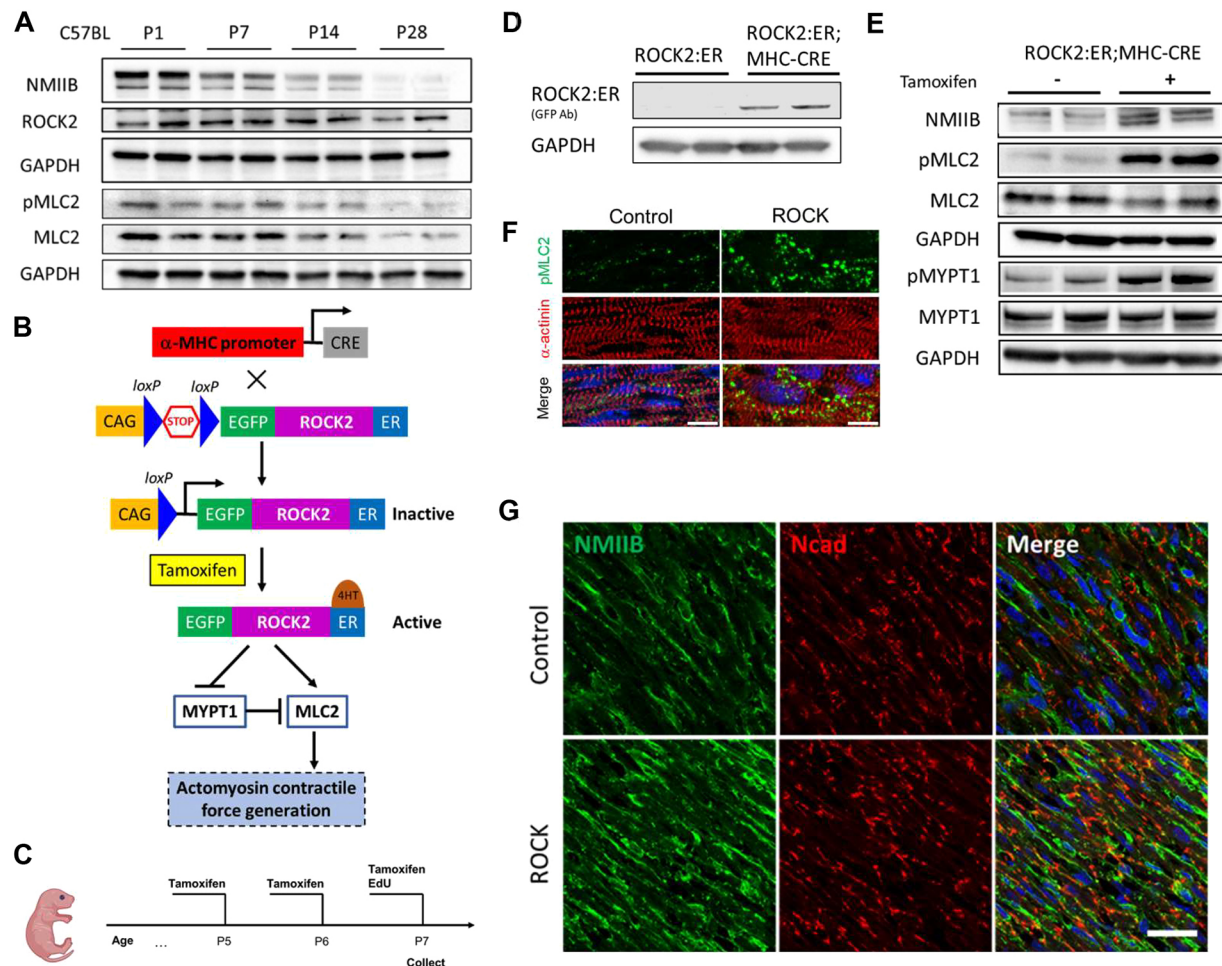
DEVELOPMENT

Fig. 1. Activation of ROCK2 kinase activity in the postnatal heart. (A) Western blot of NM IIB, ROCK2, pMLC2, MLC2 expression in C57BL/6J wild-type mice (*n*=2 hearts/time point) at P1, P7, P14 and P28. (B) Schematic of the bitransgenic mouse model consisting of a cardiac-specific Cre transgene and lox-STOP-lox ROCK2:ER transgene. The conditionally active ROCK2:ER fusion protein is inactive in the absence of ligand. Upon stimulation with Tam, the specific activity of the kinase domain of ROCK2 increases leading to phosphorylation of various substrates, which results in the generation of actomyosin contractile force. (C) Experiment timeline used to induce ROCK2 activation in CMs. Created with BioRender.com. (D) Western blot of ROCK2:ER expression (GFP antibody) in the presence or absence of MHC-Cre (*n*=2 hearts/condition). (E) Western blot analysis of NM IIB, pMLC2, MLC2, pMYPT1, MYPT1 expression in P5 hearts from ROCK2:ER mice before and after Tam activation (*n*=2 hearts/condition). (F) Representative immunofluorescence images (reconstructed from *z*-stack images) of heart sections from control and ROCK mice (*n*=3 hearts/genotype) co-stained with pMLC2 (green) and α-actinin (red). Scale bars: 10 μm. (G) Representative immunofluorescence images of heart sections of control and ROCK2:ER mice (*n*=3 hearts/genotype) co-stained with NM IIB (green) and N-cadherin (Ncad; red). Scale bar: 25 μm.

extrinsic mechanical forces (Bays and DeMali, 2017). As a mechanosensitive protein, vinculin undergoes a conformational change in response to mechanical force that results in actin remodeling and adhesion strengthening at cell junctions, a prerequisite for cadherin junction maturation. The junction remodeling process requires phosphorylation of vinculin at tyrosine residue 822 by the nonreceptor tyrosine kinase c-Abl (Abl1) (Bays et al., 2014). Thus, increased levels of vinculin phosphorylation (Y822) correlate with less mature cadherin junctions. To investigate vinculin (VCL) activity following ROCK activation, we performed immunofluorescence and western blot analyses on P7 hearts using a phospho-specific antibody that recognizes pVCL-Y822 (Bays et al., 2014). Vinculin was primarily localized at the membrane as expected, whereas phosphorylated VCL (pVCL) exhibited a diffuse but heterogeneous distribution, which was enhanced in ROCK hearts compared with control (Fig. 3A,C). Western blot analysis confirmed the increased pVCL in ROCK hearts (Fig. 3B). A portion of the pVCL

colocalized with N-cadherin at the membrane (Fig. 3C, arrowheads); however, most remained diffuse in the cytosol. Total VCL and N-cadherin protein levels did not change in ROCK hearts (Fig. 3B,D). These results are consistent with the previous observation that pharmacological inhibition of ROCK blocks force-induced VCL phosphorylation in cultured epithelial cells (Bays et al., 2014). We previously demonstrated that simultaneous depletion of both αE- and αT-catenin results in perturbation of nascent N-cadherin junctions, Rho activation and enhanced actomyosin contractility (Vite et al., 2018). Indeed, we found that pVCL expression was increased in the αE-/αT-catenin double knockout CMs (Fig. S3), comparable to observations in the ROCK model, providing independent support for pVCL as a marker of dynamic junction remodeling in the postnatal heart.

To investigate the N-cadherin/catenin complex, heart sections were co-stained with N-cadherin and either β-catenin, αE-catenin or αT-catenin. The expression and distribution of the N-cadherin/catenin adhesion complex appeared to be similar between ROCK
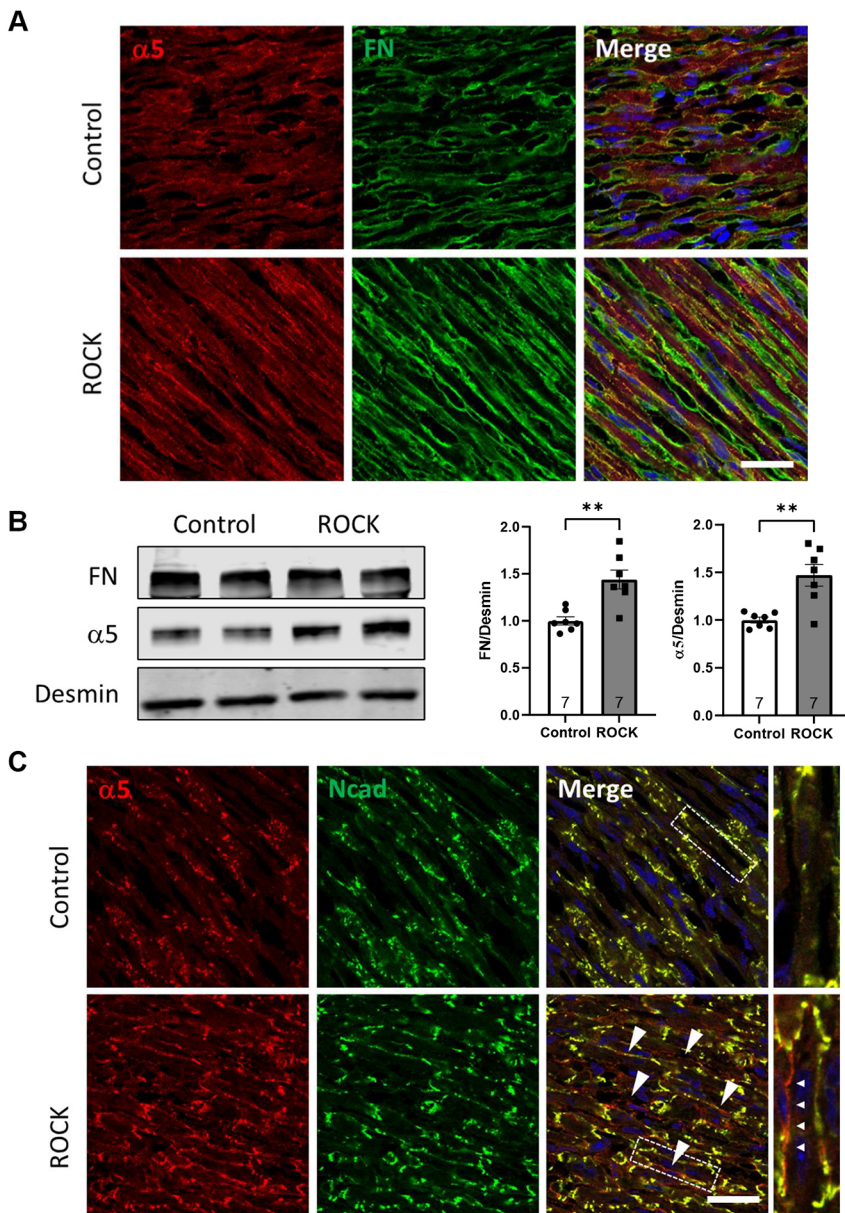
Fig. 2. Increased cellular tension leads to enhanced CM α5 integrin–FN interactions. (A) Representative immunofluorescence images of heart sections from control and ROCK P7 mice (*n*=3 hearts/genotype) co-stained for α5 integrin (red) and FN (green). (B) zWestern blot and quantitative analysis of α5 integrin and FN expression in heart tissue lysate (DOC insoluble fraction) from control (*n*=7) and ROCK (*n*=7) P7 mice. Desmin served as a loading control. (C) Representative immunofluorescence images of heart sections from control and ROCK P7 mice (*n*=3 hearts/genotype) co-stained with α5 integrin (red) and N-cadherin (Ncad; green). Arrowheads indicate increased lateral α5 integrin expression. Boxed areas are enlarged on the right. **P<0.01 (two-tailed, unpaired Student's *t*-test). Error bars represent s.e.m. Scale bars: 25 μm.

and control P7 hearts (Fig. S4). Cadherin junctions mechanically couple to the actomyosin network via mechanosensing proteins, including VCL and catenins (Lecuit and Yap, 2015); therefore, we examined VCL with either β-catenin, αE-catenin or αT-catenin. The colocalization pattern of VCL and catenins was similar between ROCK and control P7 hearts (Fig. S5). Although expression and distribution of the N-cadherin/catenin complex appeared normal, the increase VCL Y822 phosphorylation suggests that cell–cell adhesions are more dynamic and less stable in ROCK-activated CMs.

ROCK activation drives Yap nuclear translocation and increased CM proliferation

The tissue microenvironment plays a key role in the fate and function of CMs. FN and ECM-associated growth factors are crucial regulators of CM proliferation and behavior (Ieda et al., 2009; Wu et al., 2020). Therefore, we examined incorporation of 5-ethynyl-2'-deoxyuridine (EdU; an indicator of S phase) and phosphorylation of histone H3 (pHH3; an indicator of M phase) in ROCK hearts at P7 (Fig. 4A,B). No increase in cell cycle activity was observed

in control mice: ROCK alone, ROCK; MHC-Cre without Tam administration or ROCK alone plus Tam (Fig. S6). The percentage of EdU-positive CMs in ROCK hearts (10.66%±0.70%, *n*=12) was about 1.5-fold higher than in control (6.90%±0.51%, *n*=10, *P*<0.001) P7 hearts. Similarly, the percentage of pHH3-positive CMs in ROCK hearts (8.48%±0.61%, *n*=11) was about 1.9-fold higher than in control (4.50%±0.24%, *n*=11, *P*<0.0001) P7 hearts. Myocyte cross-sectional areas were reduced in the ROCK hearts (−12%; *n*=4, *P*<0.01; Fig. S7).

Mechanical cues, including rearrangement of cytoskeletal tension, control Yap activity independently of the Hippo kinase cascade (Dupont et al., 2011), and, importantly, Yap has been shown to be necessary and sufficient for CM proliferation (von Gise et al., 2012; Xin et al., 2013). Therefore, we examined the cellular distribution of Yap after activation of actomyosin contractility (Fig. 4C). Quantitative analysis demonstrated that the ROCK hearts had a 1.6-fold increase percentage of nuclear Yap-positive CMs (52.97%±2.93%, *n*=11) compared with control littermates (33.61%±2.23%, *n*=11, *P*<0.0001). There was a modest increase in
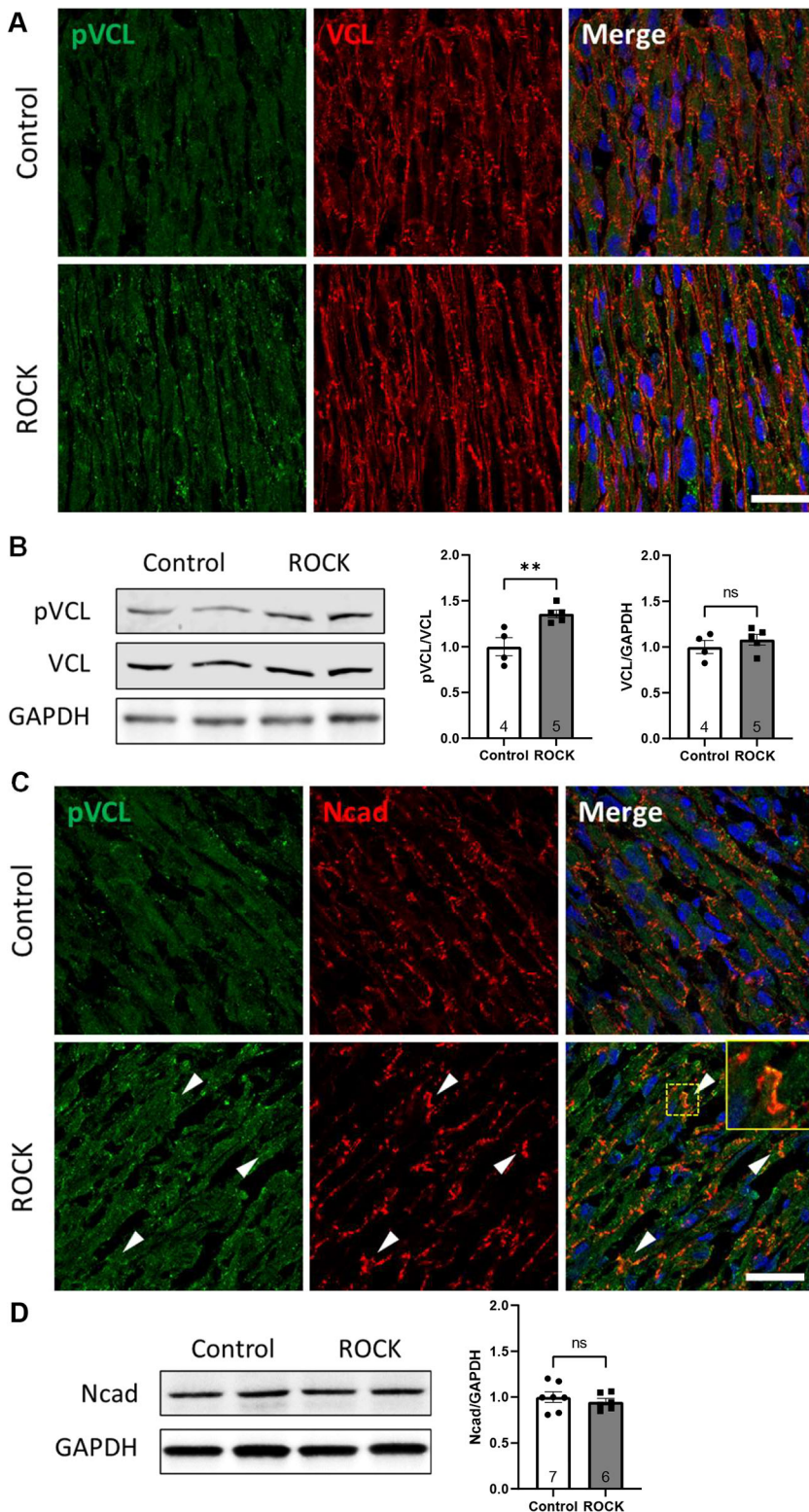
Fig. 3. Increased VCL phosphorylation following ROCK activation. (A) Representative immunofluorescence images of heart sections from control and ROCK P7 mice (*n*=3 hearts/genotype) co-stained for pVCL-Y822 (green) and VCL (red). (B) Western blot and quantitative analysis of pVCL and VCL expression in heart tissue lysate from control (*n*=4) and ROCK (*n*=5) P7 mice. (C) Representative immunofluorescence images of heart sections from control and ROCK P7 mice (*n*=3 hearts/genotype) co-stained for pVCL-Y822 (green) and N-cadherin (Ncad; red). pVCL staining was diffuse throughout the cytosol and colocalized with N-cadherin at the membrane (arrowheads, inset). (D) Western blot and quantitative analysis of N-cadherin expression in heart tissue lysate from control (*n*=7) and ROCK (*n*=6) P7 mice. ns, not significant. **P<0.01 (two-tailed, unpaired Student's *t*-test). Error bars represent s.e.m. Scale bar: 25 µm.

total Yap in ROCK hearts, but no change in phosphorylated Yap (S112 or Y357) (Fig. 4D). Next, we examined expression of Yap target genes by quantitative reverse transcription polymerase chain reaction (qRT-PCR). The Yap target genes *Ctgf* (*Ccn2*) and *Cyr61* (*Ccn1*) were upregulated twofold, consistent with increased Yap transcriptional activity in the ROCK hearts (Fig. 4E). Together, these data indicate that increasing actomyosin cytoskeletal tension is

sufficient to drive Yap to the nucleus and increase cell cycle activity, supporting a role for nonmuscle myosin contractility in the regulation of CM proliferation in the postnatal heart.

Clonal analysis in mosaic ROCK hearts

To investigate CM proliferation further, we took advantage of the integration of the loxP-STOP-loxP-EGFP:ROCK2:ER transgene at
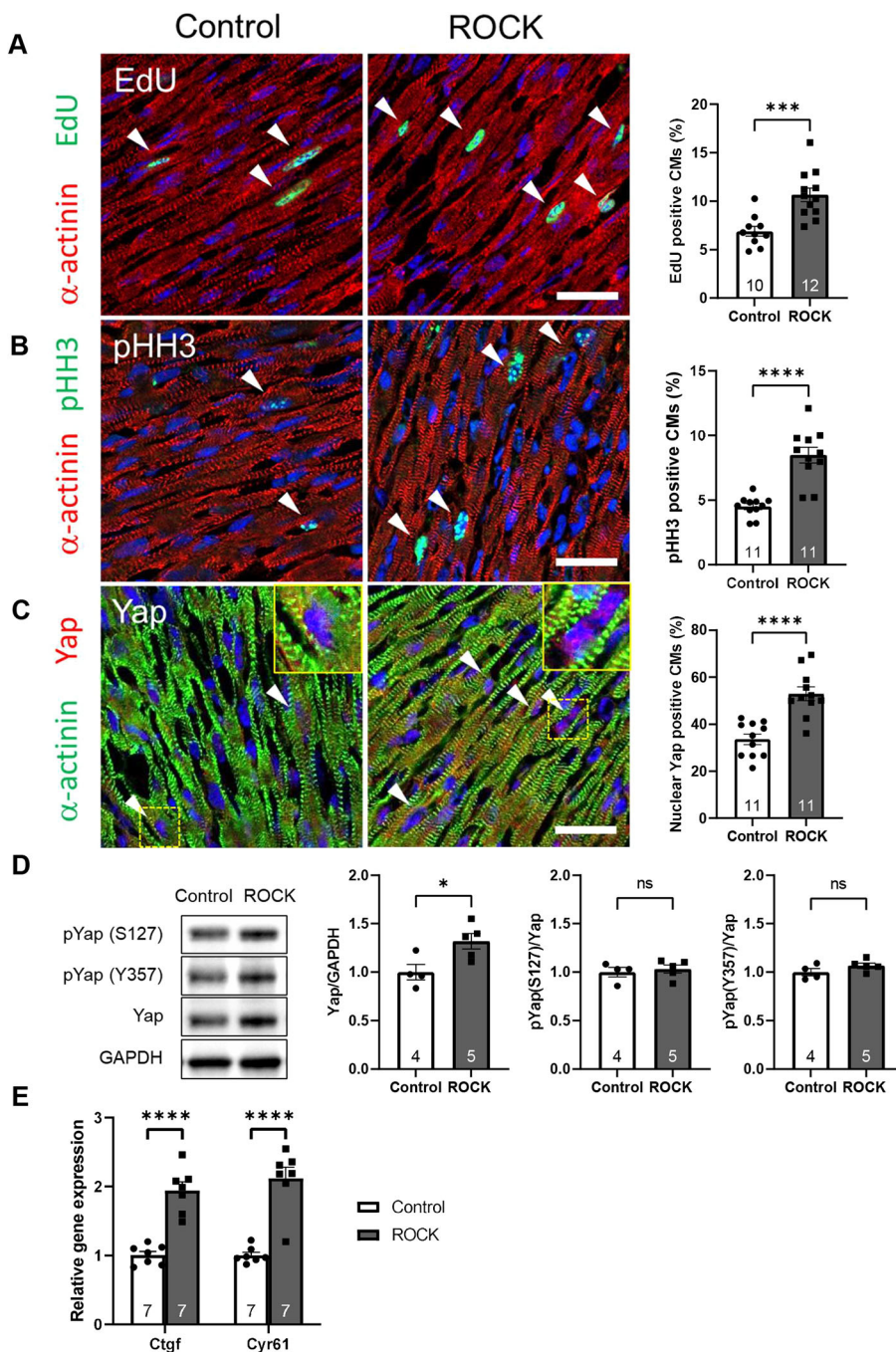
Fig. 4. ROCK activation drives Yap nuclear translocation and increased CM cell cycle activity. (A-C) Representative immunofluorescence images and quantification of heart sections from control and ROCK P7 mice (n=10-12 hearts/condition) co-stained with EdU (green)/α-actinin (red) (A), pHH3 (green)/α-actinin (red) (B) and Yap (red)/α-actinin (green) (C). Arrowheads indicate EdU-, pHH3- or nuclear Yap-positive CMs. Insets show higher magnification of the boxed areas. (D) Western blot and quantitative analysis of pYap (S127), pYap (Y357) and total Yap expression in heart tissue lysate from control (n=4), and ROCK (n=5) P7 mice. (E) Yap target gene expression assessed by qRT-PCR in control (n=7) and ROCK (n=7) P7 hearts. ns, not significant. *P<0.05, ***P<0.001; ****P<0.0001 (two-tailed, unpaired Student's t-test). Error bars represent s.e.m. Scale bars: 25 μm.

the hypoxanthine phosphoribosyltransferase (*Hprt*) locus on the X chromosome (Samuel et al., 2016). In female mammals, dosage compensation of X-linked genes between males and females occurs by genetic inactivation of one of the two X chromosomes (Goto and Monk, 1998). The choice of X chromosome to be inactivated is random in female somatic cells. We hypothesized that ROCK-activated CMs will undergo increased cell division resulting in large GFP-positive clones containing a high percentage of EdU-positive, GFP-positive CMs. To generate mosaic X^RX, MHC-Cre females, we bred MHC-Cre male mice with ROCK2:ER (R) homozygous (X^RX^R) females (Fig. 5A). The experiment is outlined in Fig. 5B. The fusion of GFP to the ROCK kinase domain enabled the identification of GFP-positive CMs using an anti-GFP antibody. In the absence of MHC-Cre, the loxP-STOP-loxP-EGFP:ROCK2:

ER transgene is not expressed. Hence, CMs exhibited no GFP signal (Fig. 5C), whereas the presence of MHC-Cre in male ROCK (X^RY) mice resulted in GFP expression in all CMs (Fig. 5C). Next, we examined GFP-positive clones in mosaic (X^RX) female hearts with and without Tam treatment (Fig. 5D). In ROCK-activated (+Tam) female (X^RX) hearts, CM clones consisted of more GFP-positive CMs compared with control (−Tam) GFP-positive clones. Importantly, the percentage of EdU-positive, GFP-positive CMs/ clone was greater in ROCK hearts compared with control female X^RX hearts. Wheat germ agglutinin (WGA) was used to stain the cell borders. The close proximity of mononucleated EdU-positive CMs is consistent with cell division and the formation of two daughter cells in ROCK-activated hearts (Fig. 5E). Taken together, these results indicate that activation of ROCK and consequent
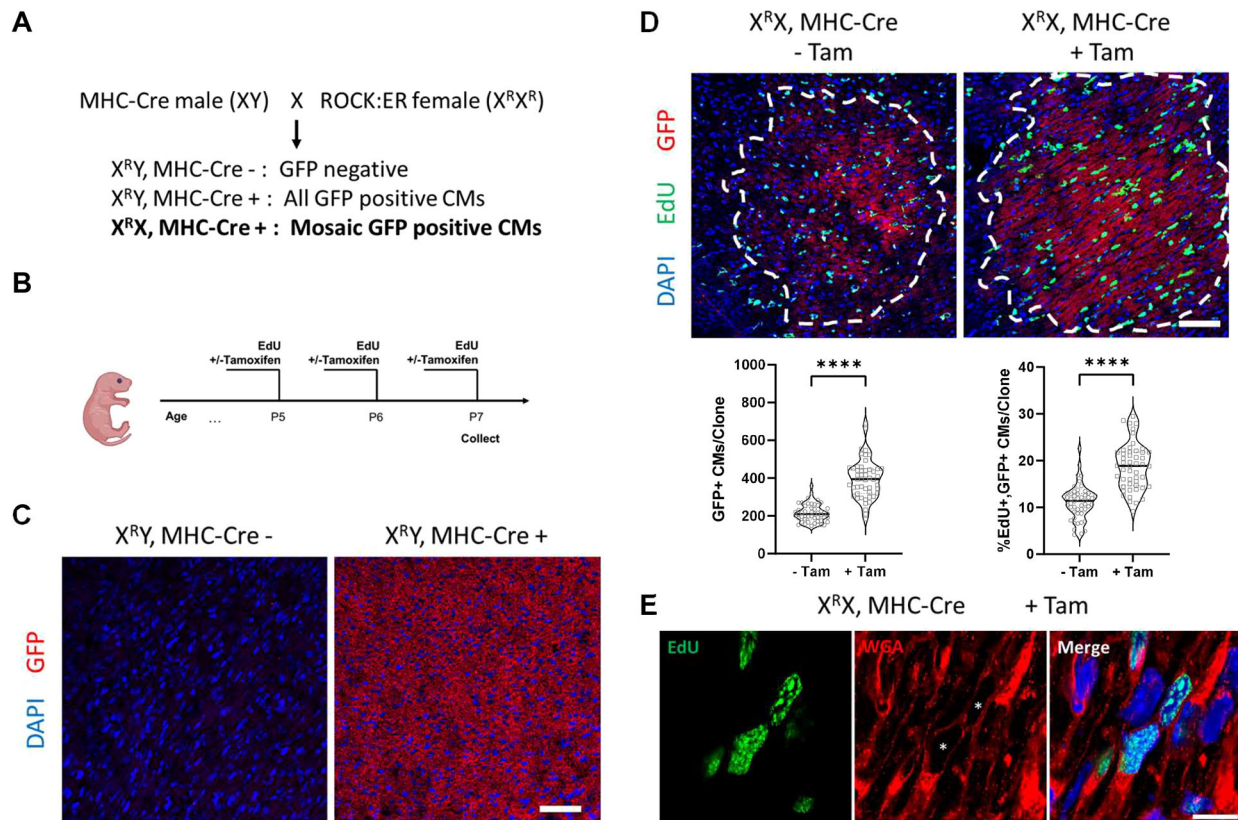
Fig. 5. Clonal analysis in mosaic female ROCK hearts. (A) Breeding scheme to generate heterozygous ROCK2:ER; MHC-Cre female mice (X^{R}X). (B) Outline of clonal analysis experiment. Created with BioRender.com. (C) Representative immunofluorescence images of heart sections from Cre – (negative control) and Cre+ male (X^{R}Y) (positive control) stained for GFP (red). Scale bar: 50 µm. (D) Representative immunofluorescence images and quantification of heart sections from heterozygous ROCK female mice with and without Tam co-stained with GFP (red) and EdU (green). The white dashed line delineates the area containing GFP-positive clones. A total number of 50 clones/group were analyzed (n=5 hearts/group). Scale bar: 50 µm. ****P<0.0001 (two-tailed, unpaired Student's t-test). Error bars represent s.e.m. (E) Representative image of a ROCK heart section stained for EdU (green) and WGA (red), a cell membrane marker. Asterisks mark WGA$^+$, EdU$^+$ mononucleated CMs. Scale bar: 10 µm. A total number of 50 clones/group were analyzed (n=5 hearts/group).

actomyosin contractility is sufficient to stimulate CM proliferation in the postnatal heart.

CM–FN interactions are required for the proliferation phenotype in ROCK2:ER hearts

ECM and ECM-associated proteins play a crucial role in regulating CM proliferation (Ieda et al., 2009; Wu et al., 2020). To determine whether CM–FN interactions are required for the hyperproliferation phenotype in the ROCK hearts, we introduced an α5 integrin (*Itga5*) floxed allele into the ROCK2:ER model to generate ROCK2:ER; *Itga5 f/+*; MHC-Cre (ROCK; α5$^{+/-}$) and ROCK2:ER; *Itga5 f/+* (control) mice (Fig. 6A). Deletion of one copy of *Itga5* resulted in reduced α5 integrin membrane expression in ROCK; α5$^{+/-}$ CMs (Fig. 6B). Consistent with knockdown of α5 integrin, FN matrix surrounding the ROCK; α5$^{+/-}$ CMs was reduced (Fig. 6B). Western blot analysis confirmed reduction of α5 integrin in ROCK; α5$^{+/-}$ heart lysates (Fig. 6C).

Next, we compared CM proliferation rates of ROCK2:ER; *Itga5 f/+* (control), ROCK2:ER; MHC-Cre (ROCK) and ROCK2:ER; *Itga5 f/+*; MHC-Cre (ROCK; α5$^{+/-}$) mice (Fig. 7A,B). The percentage of EdU-positive CMs in ROCK hearts (9.25%±0.57, n=7) was significantly higher compared with control (4.82% ±0.76%, n=4, P<0.001) and ROCK; α5$^{+/-}$ hearts (6.78%±0.32%, n=7, P<0.01) at P7. In addition to using sarcomeric α-actinin to identify CMs, EdU analysis was performed with the nuclear CM marker Nkx2-5 (Fig. S8). Comparable EdU results were obtained

with either CM marker. Similarly, the percentage of pHH3-positive CMs in ROCK hearts (7.56%±0.09%, n=6) was increased significantly compared with control (5.31%±0.12%, n=4, P<0.001) and ROCK; α5$^{+/-}$ hearts (6.01%±0.35%, n=7, P<0.01) at P7, whereas EdU and pHH3 were not significantly different between ROCK; α5$^{+/-}$ and control hearts. Thus, deletion of one copy of *Itga5* was sufficient to rescue the excessive mitotic CMs in the ROCK hearts. Next, we assessed Yap cellular distribution in the rescued hearts. Indeed, nuclear translocation of Yap was reduced in ROCK hearts upon deletion of one *Itga5* allele (Fig. 7C). The percentage of nuclear Yap-positive CMs in ROCK hearts (56.62%±2.73%, n=6) was increased significantly compared with control (31.23%±2.27%, n=4, P<0.001) and ROCK; α5$^{+/-}$ CMs (43.49%±3.62%, n=7, P<0.05) at P7, whereas the percentage of nuclear Yap positive CMs was not significantly different between ROCK; α5$^{+/-}$ and control hearts. Additionally, CM cytokinesis, as determined by Aurora-B kinase (AURKB) localization to the midbody, was increased in the ROCK (6.53 AURKB+CMs/field, n=7, P<0.001) compared with control (3.93 AURKB+CMs/field, n=4) and ROCK; α5$^{+/-}$ (3.88 AURKB+CMs/field, n=7) hearts (Fig. 7D). Collectively, our results demonstrate that high nonmuscle myosin contractility shifts the balance from cell–cell to cell–matrix adhesion, leading to Yap nuclear translocation and CM proliferation (Fig. 8). Furthermore, the effect of genetic knockdown of *Itga5* supports the proposition that CM–ECM interactions (i.e. α5/β1–FN) regulate Yap activity and CM proliferation in the postnatal ROCK heart.
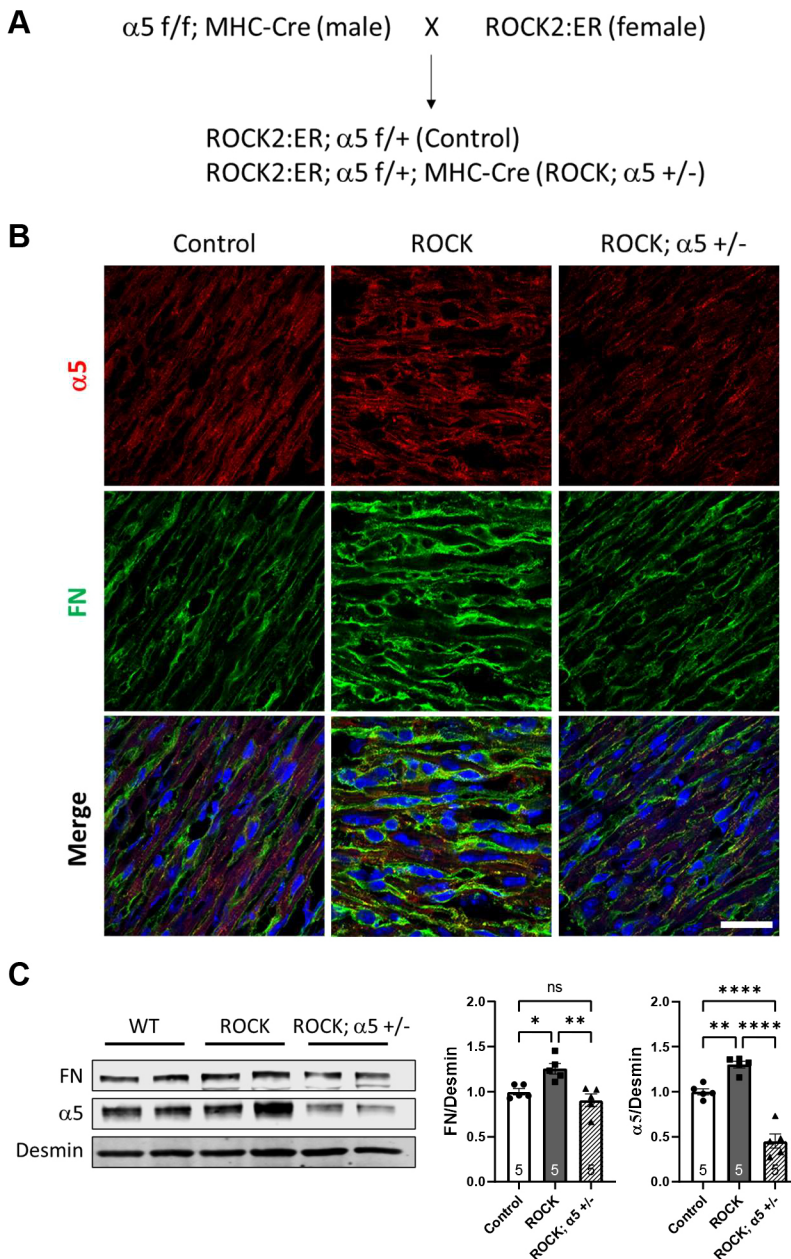
Fig. 6. CM α5 integrin is required for increased FN matrix assembly in ROCK2:ER hearts. (A) Breeding scheme to generate ROCK2:ER; *Itga5 f*/+; MHC-Cre mice (ROCK; α5$^{+/-}$). ROCK2:ER; *Itga5 f*/+ without MHC-Cre serves as control. (B) Representative immunofluorescence images of heart sections from control, ROCK, and ROCK; α5$^{+/-}$ P7 mice (*n*=3 hearts/genotype) co-stained with α5 integrin (red) and FN (green). (C) Western blot and quantitative analysis of α5 integrin and FN expression in heart tissue lysate (DOC insoluble fraction) from control (*n*=5), ROCK (*n*=5), and ROCK; α5$^{+/-}$ (*n*=5) P7 mice. Desmin served as a loading control. ns, not significant. *P<0.05, **P<0.01, ****P<0.0001 (one-way ANOVA with Tukey's multiple comparisons). Error bars represent s.e.m. Scale bar: 25 μm.

DISCUSSION

Shortly after birth, nonmuscle myosin contractility declines as CMs mature in response to increased cardiac demand and growth during the postnatal period. During the same period, myocardial cell–ECM and cell–cell interactions reorganize, resulting in the assembly of strong cell–cell contacts comprising N-cadherin/catenin adhesion complexes. The postnatal heart thus offers a unique system to investigate how actomyosin-generated contractile force regulates cell adhesion, CM maturation and cell cycle arrest. We previously reported that modification of N-cadherin junctions as a result of α-catenin depletion was associated with increased actomyosin activity, enhanced Yap nuclear translocation and increased CM proliferation in the postnatal heart (Vite et al., 2018). Based on these findings, it was hypothesized that downregulation of nonmuscle myosin contractility might be required for proper remodeling and maturation of cadherin-based and integrin-based adhesions during postnatal heart development. Here, we utilize a cardiac-restricted

ROCK2 conditionally activated gain-of-function murine model (ROCK2:ER) to evaluate directly the consequences of actomyosin contractility on postnatal CM cell adhesions and cell cycle arrest. The Tam-activated ROCK2:ER model has been used to study the effects of cellular tension on tissue homeostasis in epidermis, mammary gland, intestine and pancreas (Boyle et al., 2020; Rath et al., 2017; Samuel et al., 2011, 2016). To our knowledge, this is the first time the ROCK2:ER model has been used to manipulate actomyosin contractility in a cell type expressing both muscle myosins and nonmuscle myosins.

We report here that activation of ROCK enhances CM–ECM interactions (i.e. α5/β1–FN), thus promoting nuclear translocation of Yap, which results in increased CM proliferation in the postnatal heart. These results are consistent with our previous studies manipulating cytoskeletal tension in cultured CMs (Vite et al., 2018). We had previously shown that activation of RhoA (CN03) is sufficient to drive Yap to the nucleus in neonatal CMs grown on
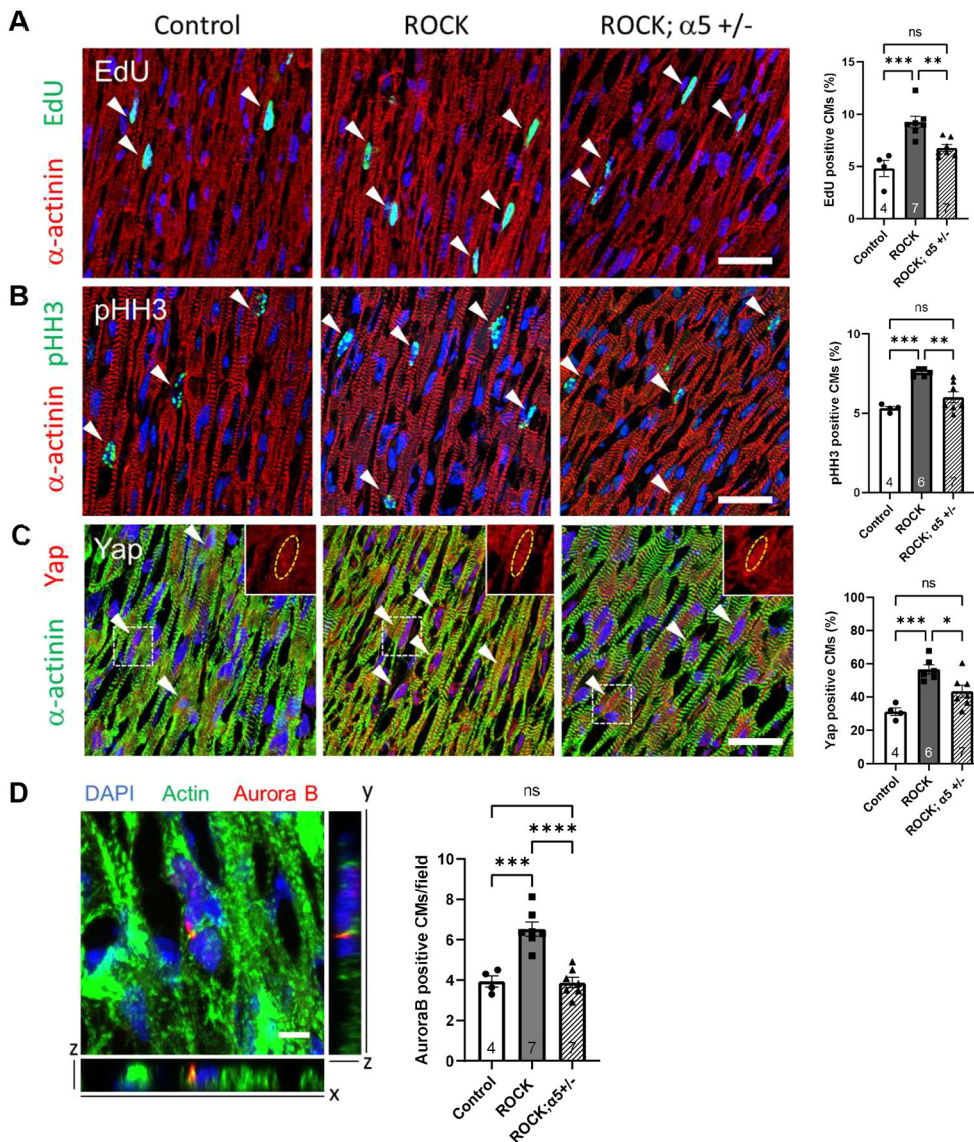
Fig. 7. CM–FN interactions are required for enhanced proliferation in ROCK2:ER mice hearts. (A-C) Representative immunofluorescence images and quantification of heart sections from control ($n=4$), ROCK ($n=6$-7) and ROCK; $\alpha5^{+/-}$ ($n=7$) P7 mice co-stained with EdU (green)/α-actinin (red) (A), pHH3 (green)/α-actinin (red) (B) and Yap (red)/α-actinin (green) (C). Arrowheads indicate EdU-, pHH3- or nuclear Yap-positive CMs. Insets show higher magnification of the boxed areas. Yellow dashed lines in insets outline nuclei. Scale bars: 25 µm. (D) Representative immunofluorescence confocal z-stack image of heart section co-stained with aurora B (red) and actin (green). Quantification of aurora B midbody staining in control ($n=4$), ROCK ($n=7$) and ROCK; $\alpha5^{+/-}$ ($n=7$) P7 mice. A minimum of ten fields (40×) per heart were analyzed. Scale bar: 5 µm. ns, not significant. *$P<0.05$, **$P<0.01$, ***$P<0.001$, ****$P<0.0001$ (one-way ANOVA with Tukey's multiple comparisons). Error bars represent s.e.m.

polyacrylamide hydrogels corresponding to physiological stiffness (Vite et al., 2018). Conversely, relieving cytoskeletal tension with pharmacological inhibitors of RhoA (CT04), ROCK (Y27632) or myosin II (blebbistatin) caused Yap to exit the nucleus (Vite et al., 2018). Moreover, RhoA activity is required for cyclic stretch-induced Yap nuclear translocation in cultured neonatal CMs (Byun et al., 2019). These *in vitro* studies support the idea that increased actomyosin contractility is responsible for Yap accumulation in the nucleus and consequent proliferation of ROCK-activated CMs.

We took advantage of X-chromosome inactivation (XCI) in mice (Lyon, 1961) to perform clonal analysis in mosaic ROCK female hearts. Transgenes targeted to the *Hprt* locus have proved useful to study XCI and its effects on regional phenotypic variability in heterozygous females (Ciavatta et al., 2006; Prosser et al., 2008; Wu et al., 2014). Using a dual fluorescent reporter system combined with a cell type-specific Cre transgene, XCI can be visualized at single-cell resolution (Wu et al., 2014). Here, we use MHC-Cre to delete the STOP signal that allows CAG-EGFP:ROCK2:ER transgene expression and CM-specific GFP signal. In ROCK (X^RY) males, all CMs express GFP, whereas heterozygous ROCK (X^RX) females exhibit a mosaic GFP staining pattern as a result of

XCI. Using EdU incorporation to mark cells in S phase, we found that ROCK activation (+Tam) leads to larger GFP$^+$ clones and, importantly, the clones consist of a higher percentage of EdU$^+$, GFP$^+$ CMs compared with control (−Tam) GFP$^+$ clones. These data further support the idea that cytoskeletal tension drives Yap to the nucleus, leading to increased CM cell cycle activity and cell division.

It is intriguing that nonmuscle myosin activity is re-activated in the adult myocardium following myocardial infarction, with pMLC found colocalized with vinculin at costameres (Pandey et al., 2018). Whether activation of actomyosin activity in the setting of ischemic injury is compensatory and beneficial remains to be determined. In support of a beneficial effect, expression of modest levels of constitutively active RhoA protected mice from ischemia/reperfusion injury, as determined by reduced infarct size and improved contractile function (Xiang et al., 2011). In the same study, RhoA loss of function resulted in worse cardiac outcome following ischemia/reperfusion injury. Thus, we can speculate that activation of nonmuscle myosin following ischemic injury may serve a dual purpose: reinforcement of cell–matrix adhesions at costameres, thus strengthening cardiac contractility, and activation
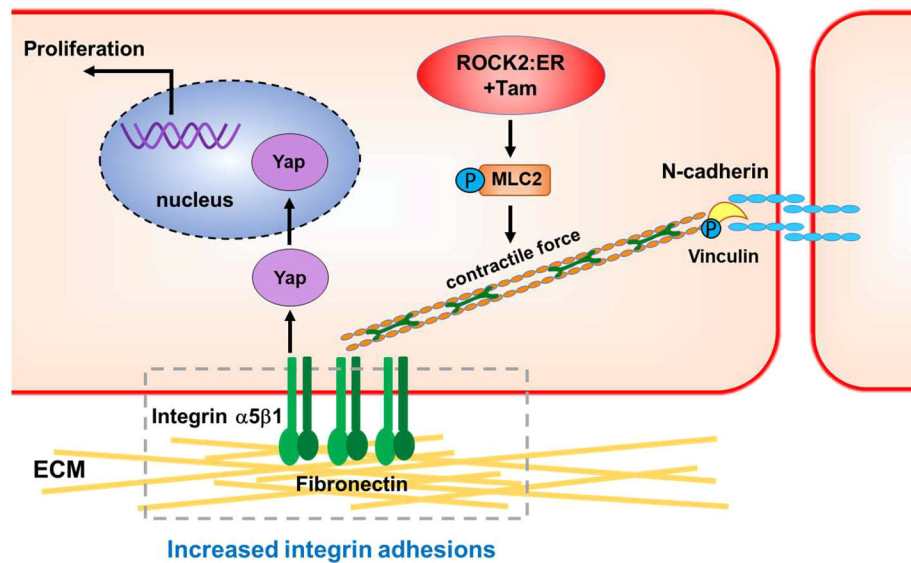
Fig. 8. Model for the role of nonmuscle myosin contractility in restricting CM proliferation. After birth, nonmuscle myosin contractility declines as muscle myosin-containing myofibrils mature and align with respect to the longitudinal axis of the CM. At the same time, expression of FN and its receptor, α5/β1, decrease in the postnatal heart. CM-specific activation of ROCK2 kinase increases actomyosin contractility, which, in turn, leads to enhanced myocyte α5/β1 integrin–FN interactions, Yap nuclear translocation, and increased CM proliferation.

of CM cell cycle activity. Future experiments will be necessary to address these and other alternative possibilities.

FN has emerged as a crucial regulator of cardiac development and myocardial growth control (Ieda et al., 2009; Mittal et al., 2013; Trinh and Stainier, 2004; Wu et al., 2020). FN matrix assembly is mediated by integrin receptors and regulated by intracellular signals, cytoskeletal organization, and availability of FN (Singh et al., 2010). Cardiac integrin α5/β1 is the primary receptor for FN. In co-culture experiments, secretion of FN by embryonic cardiac fibroblasts induces embryonic CM proliferation, which is dependent on β1 integrin signaling (Ieda et al., 2009). However, Yap activity was not investigated in this earlier study. During the postnatal period, cardiac ECM undergoes significant remodeling resulting in increased tissue stiffness (Hortells et al., 2019). FN protein levels decline 1 week after birth, as collagen levels increase and remain high in the adult myocardium. Following ischemic injury in humans, FN is re-expressed in the infarct and border zone (Willems et al., 1996). Here, we show that CM-specific activation of actomyosin contractility is sufficient to increase interstitial FN matrix. Importantly, cardiac-specific knockdown of α5 integrin (i.e. *Itga5 f/+*) reduces FN matrix and restores CM nuclear Yap and CM cell cycle activity to control levels, demonstrating that CM–FN interactions are required for enhanced CM proliferation in ROCK hearts. In cultured mesenchymal stem cells, FN-induced Yap nuclear translocation requires cytoskeletal tension (Stanton et al., 2019), consistent with our findings in ROCK-activated CMs. In postnatal CMs, Yap was shown to directly target genes involved in cytoskeletal remodeling at integrin adhesions (Morikawa et al., 2015). Moreover, Yap loss of function in nonmuscle cells leads to downregulation of α5 integrin and reduced assembly of focal adhesions (Nardone et al., 2017). In endothelium, α5 integrin/FN/ Yap mechanotransduction plays a key role in inflammation and vascular remodeling in atherosclerosis (Wang et al., 2016; Yun et al., 2019). Together, these data suggest that ROCK/integrin/Yap mechanotransduction may function as a positive-feedback loop to maintain cytoskeletal tension via cell–ECM adhesions, thus promoting Yap nuclear translocation during development and disease.

Cardiac fibroblasts (cFbs) are the major cell type contributing to the synthesis of the ECM, which surrounds the CMs and acts as a scaffold, maintaining the myocardial tissue architecture and contractile force of the heart (Hortells et al., 2019; Tallquist, 2020). Periostin (Postn) is a marker of activated cFbs, which have important roles in tissue regeneration and wound healing (Kanisicak et al., 2016). Recent lineage-tracing studies identified a heterogeneous population of cFbs in the postnatal heart consisting of Tcf21^{+} cFbs and Postn[+] cFbs (Hortells et al., 2020). Although less abundant than Tcf21^{+} cFbs, Postn[+] cFbs are highly proliferative and, importantly, their ablation during the first week leads to decreased CM mitotic activity and a reduction in binucleation. The correlation between high nonmuscle myosin activity and the appearance of Postn[+] cFbs in both the postnatal heart and in the ischemic adult heart suggest that enhanced CM intracellular tension may provide a mechanical cue to activate cFbs. Further studies are necessary to determine whether activation of actomyosin contractility is sufficient to induce Postn[+] cFbs in the heart.

Mechanosensitive proteins such as α-catenin and vinculin undergo force-induced conformational changes resulting in distinct biochemical functions, allowing cells to sense and respond to mechanical stimuli (Charras and Yap, 2018; Pannekoek et al., 2019). Although cytoskeletal tension is important for the formation of both cell–cell and cell–matrix adhesions, excessive tension might induce changes in protein conformation that lead to junctional instability (Weber et al., 2011). In the case of vinculin, site-specific tyrosine phosphorylation distinguishes its mechanical role in cadherin adhesions and integrin adhesions (Bays and DeMali, 2017). Vinculin conformational activation at cadherin-containing adherens junctions requires tension and phosphorylation at tyrosine residue Y822, which is regulated by the nonreceptor tyrosine kinase c-Abl (Bays et al., 2014; Bertocchi et al., 2017). Here, we show that ROCK activation leads to increased VCL Y822 phosphorylation, consistent with its role in force-mediated junction remodeling in epithelial cells (Bays et al., 2014). Conversely, inhibition of ROCK blocks VCL phosphorylation in epithelial cells exposed to force (Bays et al., 2014). A key avenue for future investigation will be to explore the consequences of blocking vinculin phosphorylation during N-cadherin junction remodeling in the postnatal heart.

In summary, our findings show that nonmuscle myosin contractile forces regulate the balance between myocardial cell– cell and cell–ECM adhesions, which, in turn, control Yap nuclear translocation and CM proliferation in the postnatal heart. The ability

10

to induce as well as reverse ROCK activity specifically in CMs will prove invaluable in understanding the role of cellular tension in cardiac development and regeneration, and thus provide useful insights into the potential use of actomyosin agonists for stimulating myocardial proliferation following ischemic injury.

MATERIALS AND METHODS

Generation of cardiac-restricted ROCK2:ER mouse model
Lox-Stop-Lox ROCK2:ER mice (Samuel et al., 2016), designated ROCK2: ER mice, were bred with α-Myosin heavy chain (MHC)-Cre mice (Agah et al., 1997) to generate a cardiac-restricted, conditionally-active ROCK model. α5 integrin (*Itga5*) floxed mice (van der Flier et al., 2010) were bred with MHC-Cre mice, and resulting *Itga5 f/f*; MHC-Cre mice were bred with ROCK2:ER mice to generate ROCK2:ER; *Itga5 f/+*; MHC-Cre (ROCK; α5$^{+/-}$) mice. The mice were maintained on C57BL/6J genetic background. To conditionally activate ROCK2 kinase in the postnatal heart, P5, P6 and P7 mice were injected intraperitoneally once a day with Tam (Sigma-Aldrich, T5648) at 80 mg/kg body weight. To ensure inclusion of both sexes for these studies, the sex of the neonatal pups was confirmed by the presence or absence of the Y chromosome by PCR. All animal studies were performed in accordance with the guidelines of the Institutional Animal Care and Use Committee of Rhode Island Hospital.

Echocardiographic and hemodynamic measurements
Transthoracic echocardiography was performed without anesthesia and with mice lightly restrained in a supine position, at ambient temperatures >25°C, using VisualSonics Vevo 2100 ultrasound system (FUJIFILM VisualSonics Inc.) (Fatkin et al., 1999). Two-dimensional images were obtained using a MS700 transducer (50 MHz). Heart rate, ejection fraction, fractional shortening, left ventricular internal dimensions, left ventricular volume, LVPW and LVAW, were measured from M-mode images at the plane bisecting the papillary muscles. The researcher was blinded to the genotype of the pups.

Histological analysis
Mouse hearts were isolated and washed in PBS. The hearts were then fixed in fresh 4% paraformaldehyde at 4°C overnight, dehydrated, and embedded in paraffin. Longitudinal 5-μm deparaffinized sections were stained with Hematoxylin and Eosin, mounted and imaged with Olympus BX43 microscope system. Images were elaborated with cellSens™ imaging software.

Immunofluorescence
Heart tissues were harvested 4 h after the third and final Tam injection and embedded in OCT (Sakura Finetek). OCT sections (6 μm) were fixed in 4% paraformaldehyde for 10 min and then washed in PBS three times. The heart sections were then permeabilized in 0.1% Triton X-100 (in PBS) for 10 min at room temperature. Sections were blocked by T-BSA (5% BSA in 0.01% Triton X-100 in PBS) for 1 h at room temperature and incubated overnight at 4°C with primary antibodies: pHH3 (1:200, 06-570, Millipore), YAP (1:200, 4912, Cell Signaling Technology), α-actinin (1:400, A7732, Sigma-Aldrich), N-cadherin (1:400, 610921, BD Biosciences), pMLC2 (1:100, 3674, Cell Signaling Technology), myosin IIb (1:200, M7939, Sigma-Aldrich), α5 integrin (1:200, 553319, BD Biosciences), FN (1:100, PA1-23693, Thermo Fisher Scientific), phospho-VCL-Y822 (pVCL) (1:200, ab61071, Abcam), VCL (1:100, V4505, Sigma-Aldrich), Aurora B (1:400, 611082, BD Biosciences), cardiac actin (1:400, A2103, Sigma-Aldrich), Nkx2-5 (1:200, ab35842, Abcam), αE-catenin (1:50, 711200, Invitrogen), αT-catenin (1:100, 13974-1-AP, Proteintech), β-catenin (1:200, C2206, Sigma-Aldrich). For detection of GFP, OCT sections were fixed in methanol and incubated overnight at 37°C with primary antibody (1:400, 632593, Takara Bio). After washing in PBS, sections were incubated with secondary antibodies (Alexa Fluor 488 goat anti-rabbit, A11008; Alexa Fluor 488 goat anti-mouse IgG, A11001; Alexa Fluor 555 donkey anti-mouse IgG, A31570; or Alexa Fluor 586 donkey anti-rat IgG, A175475; Life Technologies) for 1 h at room temperature. Finally, the tissue sections were washed in PBS and mounted with ProLong Gold Antifade Reagent

containing DAPI (P36935, Life Technologies). Images were acquired using a Nikon A1R confocal microscope system. z-stack images were acquired in a range of 5 μm with a step of 0.36 μm. Images were elaborated and analyzed using Nikon NIS-Elements software and ImageJ 1.53 software.

Monitoring DNA synthesis with EdU labeling
To assess CM proliferation in heart tissue, mice were injected intraperitoneally with EdU (20 mg/kg body weight) at P7. Four hours after the injection, the hearts were removed, washed in PBS, and embedded in OCT. DNA synthesis was revealed using the Click-iT EdU Alexa Fluor 488 Imaging Kit (C10337, Life Technologies) following the manufacturer's instructions and then co-stained with the cardiac marker α-actinin (1:400, A7732, Sigma-Aldrich). A minimum of ten fields at 40× with a total number of >4000 CMs per animal were analyzed.

Western blot analysis
The harvested mice heart tissues were homogenized in a modified RIPA buffer (50 mM Tris-HCl pH 7.5, 150 mM NaCl, 1 mM EDTA pH 8.0, 1% NP-40, 0.5% sodium deoxycholate, 0.1% SDS) or SDS-Urea buffer (for the detection of MLC2 and phospho-MLC2; 1% SDS, 8 mM urea, 10 mM Tris pH 7.5, 140 mM NaCl, 5 mM EDTA, 2 mM EGTA), containing protease inhibitor (11697498001, Roche Diagnostics) and phosphatase inhibitor cocktails II and III (P5726 and P0044, Sigma-Aldrich). After rotating at 4°C for 2 h, the mixtures were centrifuged at 13,000 *g* for 15 min at 4°C. Primary antibodies used were: phospho-MLC2 (1:1000, 3674, Cell Signaling Technology), MLC2 (1:1000, 3672, Cell Signaling Technology), myosin IIb (1:1000, M7939, Sigma-Aldrich), ROCK2 (1:1000, HPA007459, Sigma-Aldrich Atlas Antibodies), GFP phospho-MYPT1 (1:1000, ABS45, Millipore), MYPT1 (1:1000, 612164, BD Biosciences), α5 integrin (1:200, sc-166681, Santa Cruz Biotechnology), pVCL (1:1000, ab200825, Abcam), VCL (1:1000, V4505, Sigma-Aldrich), N-cadherin (1:1000, 610921, BD Biosciences), GAPDH (1:3000, 6c5, RDI), Yap (1:1000, 4912, Cell Signaling Technology), phospho-Yap (Y357) (1:1000, ab62751, Abcam), phospho-Yap (S127) (1:1000, 4911, Cell Signaling Technology), FN (1:3000, PA1-23693, Thermo Fisher Scientific), desmin (1:1000, 32362, Abcam). For normalization of signals, blots were also analyzed with anti-GAPDH antibody followed by IRDye 680- or IRDye 800CW-conjugated secondary antibody (1:15,000, LI-COR). Anti-mouse-HRP (1:3000, 1706516, Bio-Rad) or anti-rabbit-HRP secondary antibodies (1:3000, 1706515, Bio-Rad) were also used and developed by SuperSignal West Pico PLUS Chemiluminescent Substrate (Thermo Scientific). Membranes were imaged with Odyssey Infrared Imaging System (LI-COR) or ChemiDoc Imaging System (Bio-Rad). Quantification was performed with Fiji ImageJ 1.53 software.

Preparation of DOC soluble and insoluble fractions
DOC soluble and insoluble fractions of harvested heart tissues were prepared by a modified method as previously reported (Wierzbicka-Patynowski et al., 2004). Briefly, fresh heart tissues were homogenized in DOC lysis buffer (Tris-HCl pH 8.8, 20 mM, EDTA 2 mM, PMSF 2 mM, iodoacetic acid 2 mM, N-ethylmaleimide 2 mM, DOC 2%) with protease inhibitors (11697498001, Roche Diagnostics), and the lysates were centrifuged at 13,000 *g* 4°C for 15 min. The supernatants were saved as the DOC soluble fraction. The pellets were re-suspended in SDS solubilization buffer (Tris-HCl pH 8.8, 20 mM, EDTA 2 mM, PMSF 2 mM, iodoacetic acid 2 mM, N-ethylmaleimide 2 mM, SDS 1%) with protease inhibitors (11697498001, Roche Diagnostics). The protein concentration of DOC soluble fractions was measured by BCA assay (23225, Thermo Fisher Scientific). DOC insoluble sample volume for SDS-PAGE is based on protein concentration in the corresponding DOC soluble fraction.

Quantification of CM cell cycle activity and Yap nuclear translocation
For quantification of EdU/pHH3/nuclear Yap-positive CMs in immunofluorescence images, a minimum of ten fields (40×) per heart were analyzed using programmed analysis functions in Nikon NIS-Element AR software (Version 5.21.03). α-Actinin served as a CM marker and DAPI

was used to stain nuclei. CMs in which Yap staining overlapped with DAPI were counted as nuclear Yap-positive CMs. CMs in which pHH3 or EdU staining overlapped with DAPI were counted as pHH3- or EdU-positive CMs. Total number of DAPI within α-actinin-positive cells was regarded as the total number of CMs. Ratios of nuclear Yap-, pHH3- and EdU- positive CMs to total CMs were calculated and plotted in GraphPad Prism 9.

For clonal analysis of mosaic female ROCK hearts, ten random clones per heart from each group (n=5 hearts/group) were imaged at 40× and analyzed using Nikon NIS-Element AR software (version 5.21.03). A contiguous GFP-positive area was traced to represent a clone. The total number of GFP-positive, DAPI-positive cells was regarded as the total number of CMs per clone. Within the GFP-positive clonal area, EdU-positive, GFP-positive, DAPI-positive CMs were counted and the percentage of EdU-positive CMs per clone was calculated and plotted in GraphPad Prism 9.

RNA extraction and qRT-PCR

Total mRNA was isolated from hearts with TRIzol (Life Technologies) and precipitated with isopropyl alcohol. The concentration of isolated mRNA was determined by NanoDrop followed by treatment with the TURBO DNA-free™ kit (Life Technologies) to remove contaminating DNA. cDNA was synthesized from 1 µg of total mRNA with the LunaScript® RT SuperMix Kit (New England Biolabs) following the manufacturer's protocol. qRT-PCR was performed using the QuantStudio™ 5 System (Thermo Fisher Scientific) and iTaq Universal SYBR® Green Supermix (Bio-Rad) according to the manufacturers' instructions. Specific primers designed for RT-PCR were as follows: GAPDH forward 5′-CATCTTC-CAGGAGCGAGACC-3′, GAPDH reverse 5′-CTCGTGGTTCACACC-CATCA-3′, CTGF forward 5′-GAACAAATGCTGTGCAGGTGA-3′, CTGF reverse 5′-TCCTGGTAGGAATCGGACCTT-3′, CYR61 forward 5′-CTGCGCTAAACAACTCAACGA-3′, CYR61 reverse 5′-GCA-GATCCCTTTCAGAGCGG-3′. For each qRT-PCR, a standard curve for each gene assay was used to account for the difference in PCR efficiencies between each assay reaction. For each target gene, raw data were normalized to *Gapdh* mRNA level expressed as $2^{-\text{deltaCt}}$.

WGA lectin staining

Paraffin-embedded samples were sectioned at 5 µm thickness. The sections were deparaffinized and stained with WGA (1:400, W11261 and W11262, Invitrogen) following the manufacturer's protocol. Fluorescent images were obtained using a Nikon A1R confocal microscope system. Images were elaborated and analyzed using Nikon NIS-Elements software.

Statistical analysis

Statistical differences were assessed by unpaired, two-tailed Student's *t*-test or one-way ANOVA followed by Tukey's multiple comparison of individual means. A $P<0.05$ was considered statistically significant.

References

Agah, R., Frenkel, P. A., French, B. A., Michael, L. H., Overbeek, P. A. and Schneider, M. D. (1997). Gene recombination in postmitotic cells. Targeted expression of Cre recombinase provokes cardiac-restricted, site-specific rearrangement in adult ventricular muscle in vivo. *J. Clin. Invest.* **100**, 169-179. doi:10.1172/JCI119509

Bailey, K. E., MacGowan, G. A., Tual-Chalot, S., Phillips, L., Mohun, T. J., Henderson, D. J., Arthur, H. M., Bamforth, S. D. and Phillips, H. M. (2019). Disruption of embryonic ROCK signaling reproduces the sarcomeric phenotype of hypertrophic cardiomyopathy. *JCI Insight* **5**, e125172. doi:10.1172/jci.insight.125172

Bays, J. L. and DeMali, K. A. (2017). Vinculin in cell-cell and cell-matrix adhesions. *Cell. Mol. Life Sci.* **74**, 2999-3009. doi:10.1007/s00018-017-2511-3

Bays, J. L., Peng, X., Tolbert, C. E., Guilluy, C., Angell, A. E., Pan, Y., Superfine, R., Burridge, K. and DeMali, K. A. (2014). Vinculin phosphorylation differentially regulates mechanotransduction at cell-cell and cell-matrix adhesions. *J. Cell Biol.* **205**, 251-263. doi:10.1083/jcb.201309092

Bertocchi, C., Wang, Y., Ravasio, A., Hara, Y., Wu, Y., Sailov, T., Baird, M. A., Davidson, M. W., Zaidel-Bar, R., Toyama, Y. et al. (2017). Nanoscale architecture of cadherin-based cell adhesions. *Nat. Cell Biol.* **19**, 28-37. doi:10.1038/ncb3456

Boyle, S. T., Poltavets, V., Kular, J., Pyne, N. T., Sandow, J. J., Lewis, A. C., Murphy, K. J., Kolesnikoff, N., Moretti, P. A. B., Tea, M. N. et al. (2020). ROCK-mediated selective activation of PERK signalling causes fibroblast reprogramming and tumour progression through a CRELD2-dependent mechanism. *Nat. Cell Biol.* **22**, 882-895. doi:10.1038/s41556-020-0523-y

Byun, J., Del Re, D. P., Zhai, P., Ikeda, S., Shirakabe, A., Mizushima, W., Miyamoto, S., Brown, J. H. and Sadoshima, J. (2019). Yes-associated protein (YAP) mediates adaptive cardiac hypertrophy in response to pressure overload. *J. Biol. Chem.* **294**, 3603-3617. doi:10.1074/jbc.RA118.006123

Charras, G. and Yap, A. S. (2018). Tensile forces and mechanotransduction at cell-cell junctions. *Curr. Biol.* **28**, R445-R457. doi:10.1016/j.cub.2018.02.003

Ciavatta, D., Kalantry, S., Magnuson, T. and Smithies, O. (2006). A DNA insulator prevents repression of a targeted X-linked transgene but not its random or imprinted X inactivation. *Proc. Natl. Acad. Sci. USA* **103**, 9958-9963. doi:10.1073/pnas.0603754103

de Rooij, J., Kerstens, A., Danuser, G., Schwartz, M. A. and Waterman-Storer, C. M. (2005). Integrin-dependent actomyosin contraction regulates epithelial cell scattering. *J. Cell Biol.* **171**, 153-164. doi:10.1083/jcb.200506152

Dupont, S., Morsut, L., Aragona, M., Enzo, E., Giulitti, S., Cordenonsi, M., Zanconato, F., Le Digabel, J., Forcato, M., Bicciato, S. et al. (2011). Role of YAP/TAZ in mechanotransduction. *Nature* **474**, 179-183. doi:10.1038/nature10137

Dzamba, B. J., Jakab, K. R., Marsden, M., Schwartz, M. A. and DeSimone, D. W. (2009). Cadherin adhesion, tissue tension, and noncanonical Wnt signaling regulate fibronectin matrix organization. *Dev. Cell* **16**, 421-432. doi:10.1016/j.devcel.2009.01.008

Fatkin, D., Christe, M. E., Aristizabal, O., McConnell, B. K., Srinivasan, S., Schoen, F. J., Seidman, C. E., Turnbull, D. H. and Seidman, J. G. (1999). Neonatal cardiomyopathy in mice homozygous for the Arg403Gln mutation in the alpha cardiac myosin heavy chain gene. *J. Clin. Invest.* **103**, 147-153. doi:10.1172/JCI4631

Goto, T. and Monk, M. (1998). Regulation of X-chromosome inactivation in development in mice and humans. *Microbiol. Mol. Biol. Rev.* **62**, 362-378. doi:10.1128/MMBR.62.2.362-378.1998

Han, M. K. L. and de Rooij, J. (2016). Converging and Unique Mechanisms of Mechanotransduction at Adhesion Sites. *Trends Cell Biol.* **26**, 612-623. doi:10.1016/j.tcb.2016.03.005

Hartmann, S., Ridley, A. J. and Lutz, S. (2015). The function of rho-associated kinases ROCK1 and ROCK2 in the pathogenesis of cardiovascular disease. *Front. Pharmacol.* **6**, 276. doi:10.3389/fphar.2015.00276

Hortells, L., Johansen, A. K. Z. and Yutzey, K. E. (2019). Cardiac fibroblasts and the extracellular matrix in regenerative and nonregenerative hearts. *J. Cardiovasc. Dev. Dis.* **6**, 29. doi:10.3390/jcdd6030029

Hortells, L., Valiente-Alandi, I., Thomas, Z. M., Agnew, E. J., Schnell, D. J., York, A. J., Vagnozzi, R. J., Meyer, E. C., Molkentin, J. D. and Yutzey, K. E. (2020). A specialized population of Periostin-expressing cardiac fibroblasts contributes to postnatal cardiomyocyte maturation and innervation. *Proc. Natl. Acad. Sci. USA* **117**, 21469-21479. doi:10.1073/pnas.2009119117

Ieda, M., Tsuchihashi, T., Ivey, K. N., Ross, R. S., Hong, T. T., Shaw, R. M. and Srivastava, D. (2009). Cardiac fibroblasts regulate myocardial proliferation through beta1 integrin signaling. *Dev. Cell* **16**, 233-244. doi:10.1016/j.devcel.2008.12.007

DEVELOPMENT

Kanisicak, O., Khalil, H., Ivey, M. J., Karch, J., Maliken, B. D., Correll, R. N., Brody, M. J., SC, J. L., Aronow, B. J., Tallquist, M. D. et al. (2016). Genetic lineage tracing defines myofibroblast origin and function in the injured heart. *Nat. Commun.* **7**, 12260. doi:10.1038/ncomms12260

Lecuit, T. and Yap, A. S. (2015). E-cadherin junctions as active mechanical integrators in tissue dynamics. *Nat. Cell Biol.* **17**, 533-539. doi:10.1038/ncb3136

Li, J., Gao, E., Vite, A., Yi, R., Gomez, L., Goossens, S., van Roy, F. and Radice, G. L. (2015). Alpha-catenins control cardiomyocyte proliferation by regulating Yap activity. *Circ. Res.* **116**, 70-79. doi:10.1161/CIRCRESAHA.116.304472

Liu, Z., Tan, J. L., Cohen, D. M., Yang, M. T., Sniadecki, N. J., Ruiz, S. A., Nelson, C. M. and Chen, C. S. (2010). Mechanical tugging force regulates the size of cell-cell junctions. *Proc. Natl. Acad. Sci. USA* **107**, 9944-9949. doi:10.1073/pnas.0914547107

Lyon, M. F. (1961). Gene action in the X-chromosome of the mouse (Mus musculus L.). *Nature* **190**, 372-373. doi:10.1038/190372a0

Ma, X. and Adelstein, R. S. (2012). In vivo studies on nonmuscle myosin II expression and function in heart development. *Front. Biosci. (Landmark Ed)* **17**, 545-555. doi:10.2741/3942

Ma, X., Takeda, K., Singh, A., Yu, Z. X., Zerfas, P., Blount, A., Liu, C., Towbin, J. A., Schneider, M. D., Adelstein, R. S. et al. (2009). Conditional ablation of nonmuscle myosin II-B delineates heart defects in adult mice. *Circ. Res.* **105**, 1102-1109. doi:10.1161/CIRCRESAHA.109.200303

Ma, X., Kovacs, M., Conti, M. A., Wang, A., Zhang, Y., Sellers, J. R. and Adelstein, R. S. (2012). Nonmuscle myosin II exerts tension but does not translocate actin in vertebrate cytokinesis. *Proc. Natl. Acad. Sci. USA* **109**, 4509-4514. doi:10.1073/pnas.1116268109

Martinez-Rico, C., Pincet, F., Thiery, J. P. and Dufour, S. (2010). Integrins stimulate E-cadherin-mediated intercellular adhesion by regulating Src-kinase activation and actomyosin contractility. *J. Cell Sci.* **123**, 712-722. doi:10.1242/jcs.047878

Mittal, A., Pulina, M., Hou, S. Y. and Astrof, S. (2013). Fibronectin and integrin alpha 5 play requisite roles in cardiac morphogenesis. *Dev. Biol.* **381**, 73-82. doi:10.1016/j.ydbio.2013.06.010

Morikawa, Y., Zhang, M., Heallen, T., Leach, J., Tao, G., Xiao, Y., Bai, Y., Li, W., Willerson, J. T. and Martin, J. F. (2015). Actin cytoskeletal remodeling with protrusion formation is essential for heart regeneration in Hippo-deficient mice. *Sci. Signal.* **8**, ra41. doi:10.1126/scisignal.2005781

Mui, K. L., Chen, C. S. and Assoian, R. K. (2016). The mechanical regulation of integrin-cadherin crosstalk organizes cells, signaling and forces. *J. Cell Sci.* **129**, 1093-1100.

Nardone, G., Oliver-De La Cruz, J., Vrbsky, J., Martini, C., Pribyl, J., Skladal, P., Pesl, M., Caluori, G., Pagliari, S., Martino, F. et al. (2017). YAP regulates cell mechanics by controlling focal adhesion assembly. *Nat. Commun.* **8**, 15321. doi:10.1038/ncomms15321

Noma, K., Oyama, N. and Liao, J. K. (2006). Physiological role of ROCKs in the cardiovascular system. *Am. J. Physiol. Cell Physiol.* **290**, C661-C668. doi:10.1152/ajpcell.00459.2005

Okamoto, R., Li, Y., Noma, K., Hiroi, Y., Liu, P. Y., Taniguchi, M., Ito, M. and Liao, J. K. (2013). FHL2 prevents cardiac hypertrophy in mice with cardiac-specific deletion of ROCK2. *FASEB J.* **27**, 1439-1449. doi:10.1096/fj.12-217018

Pandey, P., Hawkes, W., Hu, J., Megone, W. V., Gautrot, J., Anilkumar, N., Zhang, M., Hirvonen, L., Cox, S., Ehler, E. et al. (2018). Cardiomyocytes sense matrix rigidity through a combination of muscle and non-muscle myosin contractions. *Dev. Cell* **44**, 326-336.e323. doi:10.1016/j.devcel.2017.12.024

Pannekoek, W. J., de Rooij, J. and Gloerich, M. (2019). Force transduction by cadherin adhesions in morphogenesis. *F1000Res* **8**, F1000. doi:10.12688/f1000research.18779.1

Porrello, E. R., Mahmoud, A. I., Simpson, E., Hill, J. A., Richardson, J. A., Olson, E. N. and Sadek, H. A. (2011). Transient regenerative potential of the neonatal mouse heart. *Science* **331**, 1078-1080. doi:10.1126/science.1200708

Porrello, E. R., Mahmoud, A. I., Simpson, E., Johnson, B. A., Grinsfelder, D., Canseco, D., Mammen, P. P., Rothermel, B. A., Olson, E. N. and Sadek, H. A. (2013). Regulation of neonatal and adult mammalian heart regeneration by the miR-15 family. *Proc. Natl. Acad. Sci. USA* **110**, 187-192. doi:10.1073/pnas.1208863110

Prosser, H. M., Rzadzinska, A. K., Steel, K. P. and Bradley, A. (2008). Mosaic complementation demonstrates a regulatory role for myosin VIIa in actin dynamics of stereocilia. *Mol. Cell. Biol.* **28**, 1702-1712. doi:10.1128/MCB.01282-07

Rath, N., Morton, J. P., Julian, L., Helbig, L., Kadir, S., McGhee, E. J., Anderson, K. I., Kalna, G., Mullin, M., Pinho, A. V. et al. (2017). ROCK signaling promotes collagen remodeling to facilitate invasive pancreatic ductal adenocarcinoma tumor cell growth. *EMBO Mol. Med.* **9**, 198-218. doi:10.15252/emmm.201606743

Samuel, M. S., Lopez, J. I., McGhee, E. J., Croft, D. R., Strachan, D., Timpson, P., Munro, J., Schroder, E., Zhou, J., Brunton, V. G. et al. (2011). Actomyosin-mediated cellular tension drives increased tissue stiffness and beta-catenin activation to induce epidermal hyperplasia and tumor growth. *Cancer Cell* **19**, 776-791. doi:10.1016/j.ccr.2011.05.008

Samuel, M. S., Rath, N., Masre, S. F., Boyle, S. T., Greenhalgh, D. A., Kochetkova, M., Bryson, S., Stevenson, D. and Olson, M. F. (2016). Tissue-selective expression of a conditionally-active ROCK2-estrogen receptor fusion protein. *Genesis* **54**, 636-646. doi:10.1002/dvg.22988

Sechler, J. L., Takada, Y. and Schwarzbauer, J. E. (1996). Altered rate of fibronectin matrix assembly by deletion of the first type III repeats. *J. Cell Biol.* **134**, 573-583. doi:10.1083/jcb.134.2.573

Shewan, A. M., Maddugoda, M., Kraemer, A., Stehbens, S. J., Verma, S., Kovacs, E. M. and Yap, A. S. (2005). Myosin 2 is a key Rho kinase target necessary for the local concentration of E-cadherin at cell-cell contacts. *Mol. Biol. Cell* **16**, 4531-4542. doi:10.1091/mbc.e05-04-0330

Shi, J., Surma, M., Yang, Y. and Wei, L. (2019). Disruption of both ROCK1 and ROCK2 genes in cardiomyocytes promotes autophagy and reduces cardiac fibrosis during aging. *FASEB J.* **33**, 7348-7362. doi:10.1096/fj.201802510R

Shi, J., Zhang, L. and Wei, L. (2011). Rho-kinase in development and heart failure: insights from genetic models. *Pediatr. Cardiol.* **32**, 297-304. doi:10.1007/s00246-011-9920-0

Shimokawa, H., Sunamura, S. and Satoh, K. (2016). RhoA/Rho-kinase in the cardiovascular system. *Circ. Res.* **118**, 352-366. doi:10.1161/CIRCRESAHA.115.306532

Singh, P., Carraher, C. and Schwarzbauer, J. E. (2010). Assembly of fibronectin extracellular matrix. *Annu. Rev. Cell Dev. Biol.* **26**, 397-419. doi:10.1146/annurev-cellbio-100109-104020

Soonpaa, M. H., Kim, K. K., Pajak, L., Franklin, M. and Field, L. J. (1996). Cardiomyocyte DNA synthesis and binucleation during murine development. *Am. J. Physiol.* **271**, H2183-H2189.

Stanton, A. E., Tong, X., Lee, S. and Yang, F. (2019). Biochemical ligand density regulates yes-associated protein translocation in stem cells through cytoskeletal tension and integrins. *ACS Appl. Mater Interfaces* **11**, 8849-8857. doi:10.1021/acsami.8b21270

Sunamura, S., Satoh, K., Kurosawa, R., Ohtsuki, T., Kikuchi, N., Elias-Al-Mamun, M., Shimizu, T., Ikeda, S., Suzuki, K., Satoh, T. et al. (2018). Different roles of myocardial ROCK1 and ROCK2 in cardiac dysfunction and postcapillary pulmonary hypertension in mice. *Proc. Natl. Acad. Sci. USA* **115**, E7129-E7138. doi:10.1073/pnas.1721298115

Takeda, K., Kishi, H., Ma, X., Yu, Z. X. and Adelstein, R. S. (2003). Ablation and mutation of nonmuscle myosin heavy chain II-B results in a defect in cardiac myocyte cytokinesis. *Circ. Res.* **93**, 330-337. doi:10.1161/01.RES.0000089256.00309.CB

Tallquist, M. D. (2020). Cardiac Fibroblast Diversity. *Annu. Rev. Physiol.* **82**, 63-78. doi:10.1146/annurev-physiol-021119-034527

Trinh, L. A. and Stainier, D. Y. (2004). Fibronectin regulates epithelial organization during myocardial migration in zebrafish. *Dev. Cell* **6**, 371-382. doi:10.1016/S1534-5807(04)00063-2

Tullio, A. N., Accili, D., Ferrans, V. J., Yu, Z. X., Takeda, K., Grinberg, A., Westphal, H., Preston, Y. A. and Adelstein, R. S. (1997). Nonmuscle myosin II-B is required for normal development of the mouse heart. *Proc. Natl. Acad. Sci. USA* **94**, 12407-12412. doi:10.1073/pnas.94.23.12407

van der Flier, A., Badu-Nkansah, K., Whittaker, C. A., Crowley, D., Bronson, R. T., Lacy-Hulbert, A. and Hynes, R. O. (2010). Endothelial alpha5 and alphav integrins cooperate in remodeling of the vasculature during development. *Development* **137**, 2439-2449. doi:10.1242/dev.049551

Vite, A. and Radice, G. L. (2014). N-cadherin/catenin complex as a master regulator of intercalated disc function. *Cell Commun. Adhes.* **21**, 169-179. doi:10.3109/15419061.2014.908853

Vite, A., Zhang, C., Yi, R., Emms, S. and Radice, G. L. (2018). α-Catenin-dependent cytoskeletal tension controls Yap activity in the heart. *Development* **145**, dev149823. doi:10.1242/dev.149823

von Gise, A., Lin, Z., Schlegelmilch, K., Honor, L. B., Pan, G. M., Buck, J. N., Ma, Q., Ishiwata, T., Zhou, B., Camargo, F. D. et al. (2012). YAP1, the nuclear target of Hippo signaling, stimulates heart growth through cardiomyocyte proliferation but not hypertrophy. *Proc. Natl. Acad. Sci. USA* **109**, 2394-2399. doi:10.1073/pnas.1116136109

Wang, L., Luo, J. Y., Li, B., Tian, X. Y., Chen, L. J., Huang, Y., Liu, J., Deng, D., Lau, C. W., Wan, S. et al. (2016). Integrin-YAP/TAZ-JNK cascade mediates atheroprotective effect of unidirectional shear flow. *Nature* **540**, 579-582. doi:10.1038/nature20602

Weber, G. F., Bjerke, M. A. and DeSimone, D. W. (2011). Integrins and cadherins join forces to form adhesive networks. *J. Cell Sci.* **124**, 1183-1193. doi:10.1242/jcs.064618

Wei, L., Roberts, W., Wang, L., Yamada, M., Zhang, S., Zhao, Z., Rivkees, S. A., Schwartz, R. J. and Imanaka-Yoshida, K. (2001). Rho kinases play an obligatory role in vertebrate embryonic organogenesis. *Development* **128**, 2953-2962. doi:10.1242/dev.128.15.2953

Wierzbicka-Patynowski, I., Mao, Y. and Schwarzbauer, J. E. (2004). Analysis of fibronectin matrix assembly. *Curr. Protoc. Cell Biol. Chapter* **10**, Unit 10 12.

Willems, I. E., Arends, J. W. and Daemen, M. J. (1996). Tenascin and fibronectin expression in healing human myocardial scars. *J. Pathol.* **179**, 321-325. doi:10.1002/(SICI)1096-9896(199607)179:3<321::AID-PATH555>3.0.CO;2-8

DEVELOPMENT

Wu, H., Luo, J., Yu, H., Rattner, A., Mo, A., Wang, Y., Smallwood, P. M., Erlanger, B., Wheelan, S. J. and Nathans, J. (2014). Cellular resolution maps of X chromosome inactivation: implications for neural development, function, and disease. *Neuron* **81**, 103-119. doi:10.1016/j.neuron.2013.10.051

Wu, C. C., Jeratsch, S., Graumann, J. and Stainier, D. Y. R. (2020). Modulation of mammalian cardiomyocyte cytokinesis by the extracellular Matrix. *Circ. Res.* **127**, 896-907. doi:10.1161/CIRCRESAHA.119.316303

Xiang, S. Y., Vanhoutte, D., Del Re, D. P., Purcell, N. H., Ling, H., Banerjee, I., Bossuyt, J., Lang, R. A., Zheng, Y., Matkovich, S. J. et al. (2011). RhoA protects the mouse heart against ischemia/reperfusion injury. *J. Clin. Invest.* **121**, 3269-3276. doi:10.1172/JCI44371

Xin, M., Kim, Y., Sutherland, L. B., Murakami, M., Qi, X., McAnally, J., Porrello, E. R., Mahmoud, A. I., Tan, W., Shelton, J. M. et al. (2013). Hippo pathway effector Yap promotes cardiac regeneration. *Proc. Natl. Acad. Sci. USA* **110**, 13839-13844. doi:10.1073/pnas.1313192110

Yun, S., Hu, R., Schwaemmle, M. E., Scherer, A. N., Zhuang, Z., Koleske, A. J., Pallas, D. C. and Schwartz, M. A. (2019). Integrin alpha5beta1 regulates PP2A complex assembly through PDE4D in atherosclerosis. *J. Clin. Invest.* **129**, 4863-4874. doi:10.1172/JCI127692

Zuidema, A., Wang, W. and Sonnenberg, A. (2020). Crosstalk between cell adhesion complexes in regulation of mechanotransduction. *BioEssays* **42**, e2000119. doi:10.1002/bies.202000119

DEVELOPMENT